AGU ADVANCING EARTH AND SPACE SCIENCES

Geophysical Research Letters

RESEARCH LETTER
10.1029/2024GL109446

Atmospheric River Rapids and Their Role in the Extreme Rainfall Event of April 2023 in the Middle East

Diana Francis[1], Ricardo Fonseca[1], Deniz Bozkurt[2,3], Narendra Nelli[1], and Bin Guan[4,5]

[1]Environmental and Geophysical Sciences (ENGEOS) Lab, Earth Sciences Department, Khalifa University, Abu Dhabi, United Arab Emirates, [2]Department of Meteorology, Universidad de Valparaíso, Valparaíso, Chile, [3]Center for Climate and Resilience Research (CR)2, Santiago, Chile, [4]Joint Institute for Regional Earth System Science and Engineering, University of California, Los Angeles, Los Angeles, CA, USA, [5]Jet Propulsion Laboratory, California Institute of Technology, Pasadena, CA, USA

Abstract The mesoscale dynamics of a record-breaking Atmospheric River (AR) that impacted the Middle East in mid-April 2023 and caused property damage and loss of life are investigated using model, reanalysis and observational data. The high-resolution (2.5 km) simulations revealed the presence of AR rapids, narrow and long convective structures embedded within the AR that generated heavy precipitation (>4 mm hr^{-1}) as they moved at high speeds (>30 m s^{-1}) from northeastern Africa into western Iran. Gravity waves triggered by the complex terrain in Saudi Arabia further intensified their effects. Given the rising frequency of ARs in this region, AR rapids may be even more impactful in a warming climate, and need to be accounted for in reanalysis and numerical models.

Plain Language Summary Atmospheric Rivers (ARs) are narrow and long bands of high water vapor content, which largely originate in the tropics or subtropics and propagate into mid- and high-latitudes. They can bring beneficial rain and snow but, in particular the most intense, can lead to catastrophic flooding and loss of life. One of such occurrences in the Middle East in mid-April 2023 is investigated using model and observational data. The high-resolution (2.5 km) simulation put in evidence narrow (5–15 km) and long (100–200 km) convective structures within the AR, known as AR rapids, which produced heavy precipitation (>4 mm hr^{-1}), further enhanced by gravity waves that developed over the high terrain in western Saudi Arabia, and propagated at high speeds (>30 m s^{-1}). ARs are occurring more frequently in the Middle East as they are globally, and with increased atmospheric water vapor in a warming climate, AR rapids may be even more destructive.

Key Points:

- The exceptional and impactful Atmospheric River of mid-April 2023 in the Middle East is investigated with model and observational data
- A 2.5 km simulation reveals the presence of "Atmospheric River rapids," narrow along-flow structures that generated rain rates >4 mm hr^{-1}
- Model simulations and ground-based observations underlined the effects of the Atmospheric River and associated trailing cold front

Supporting Information:

Supporting Information may be found in the online version of this article.

Correspondence to:

D. Francis,
diana.francis@ku.ac.ae

Citation:

Francis, D., Fonseca, R., Bozkurt, D., Nelli, N., & Guan, B. (2024). Atmospheric river rapids and their role in the extreme rainfall event of April 2023 in the Middle East. *Geophysical Research Letters*, *51*, e2024GL109446. https://doi.org/10.1029/2024GL109446

Received 23 MAR 2024
Accepted 26 APR 2024

Author Contributions:

Conceptualization: Diana Francis
Data curation: Ricardo Fonseca, Narendra Nelli
Formal analysis: Ricardo Fonseca, Deniz Bozkurt
Funding acquisition: Diana Francis
Methodology: Diana Francis, Ricardo Fonseca
Project administration: Diana Francis
Resources: Diana Francis
Software: Bin Guan
Supervision: Diana Francis
Validation: Ricardo Fonseca, Deniz Bozkurt, Bin Guan

1. Introduction

Atmospheric Rivers (ARs) are narrow and long filaments of moisture-rich air that typically originate in the tropics/subtropics and propagate poleward into the mid- and high-latitudes (Gimeno et al., 2014; Zhu & Newell, 1998). They are generally detected based on the associated integrated vapor transport (IVT), which is the column integral of the flux of water vapor carried by the horizontal wind flow (Guan & Waliser, 2015; Guan et al., 2023; Lora et al., 2020; Zhou et al., 2018), while their strength and impacts are typically a function of the magnitude and persistence of high IVT values (Eiras-Barca et al., 2021; Esfandiari & Rezaei, 2022; Ralph et al., 2019). ARs are associated with different time-scales, ranging from high-frequency (<10 days) predominantly over the mid-latitude storm tracks, to low-frequency in the summer monsoon regions, with intermediate ARs found on the poleward side of subtropical highs (Park et al., 2023). While in monsoon and lower latitude regions they further exacerbate rainfall events (Liang & Yong, 2021; Park et al., 2021; Vallejo-Bernal et al., 2023; Yang et al., 2018), at high-latitudes and over the high-terrain, ARs can have a substantial effect on sea-/land-ice and snow cover (Box et al., 2023; Bozkurt et al., 2021; Fonseca et al., 2023; Francis et al., 2020, 2021a, 2022a, 2022b; Meinander et al., 2023; Shields et al., 2022b; Wille et al., 2024a, 2024b; Zhang et al., 2023). When they move over a dust source region, such as the Saharan and Arabian Deserts, the associated wind flow can trigger dust lifting and create hazardous conditions (Dezfuli, 2020; Dezfuli et al., 2021; Francis et al., 2023; Nelli et al., 2021a; Voss et al., 2021). Besides water vapor and dust, ARs can transport other aerosols such as black and organic carbon and sea salt (Chakraborty et al., 2021, 2022; Lapere et al., 2024). They account for up to 50% of the wintertime precipitation in mid-latitude regions (Lavers & Villarini, 2015), and are projected to be stronger and

Visualization: Ricardo Fonseca, Narendra Nelli
Writing – original draft: Diana Francis, Ricardo Fonseca
Writing – review & editing: Diana Francis, Ricardo Fonseca, Deniz Bozkurt

more persistent in a warming climate (Espinoza et al., 2018; Massoud et al., 2020; Nellikkattil et al., 2023; Payne et al., 2020; Shields & Kiehl, 2016; Tian et al., 2023; Wang et al., 2023).

ARs in the Middle East are more frequent and the strongest in March, when about 23% of all ARs take place, and least frequent and the weakest in November, when roughly 13% occur (Esfandiari & Rezaei, 2022). This is in contrast with Europe and the United States, where ARs make landfall mostly in the colder months of October to March (Lavers & Villarini, 2015). The difference in the timing can be explained by the different mechanisms that promote the development of ARs. In Europe and the United States, they are typically associated with baroclinic weather systems, which are more active in the colder months when the pole to equator temperature difference is maximized. On the other hand, the paths of Middle East ARs are modulated by the position of the Arabian Peninsula's subtropical high (Alghamdi & Harrington Jr, 2022, 2023), the Red Sea Trough (de Vries et al., 2013, 2016), and mid-latitude troughs (Esfandiari & Lashkari, 2020; Francis et al., 2023). The Red Sea Trough is more active during spring and autumn compared to winter (Tsvieli & Zangvil, 2007), while cyclogenesis in parts of the southern Mediterranean is more frequent in spring (Flaounas et al., 2022; Lionello et al., 2016). ARs in the Middle East tend to be less intense, in terms of the associated IVT, compared to those in Europe and North America, owing to the aridity of the neighboring north Africa and Sahara (Bozkurt et al., 2021; Eiras-Barca et al., 2021; Esfandiari & Rezaei, 2022). However, their horizontal and vertical structures are similar to those of ARs elsewhere, despite regional variations in intensity and impact (e.g., Bozkurt et al., 2021; Dezfuli, 2020; Dezfuli et al., 2021; Payne et al., 2020). In terms of frequency of occurrence, ARs make landfall up to two to three times more frequently in the west coast of Europe and North America compared to the Middle East (Wang et al., 2024). Dezfuli (2020) reported on an AR in March 2019 that delivered up to 400 mm of rainfall, leading to widespread floods and loss of life in parts of Iran. The IVT exceeded 350 kg m^{-1} s^{-1}, with contributions from the tropical Atlantic, Arabian Sea and Mediterranean Sea, further enhanced as the AR moved over the Red Sea and Arabian Gulf. Dezfuli et al. (2021) and Francis et al. (2023) highlighted the role of ARs in triggering dust storms in the Middle East: in the former dust is lifted directly by the atmospheric circulation that promoted the development of the AR, while in the latter density currents emanated from deep convection fueled by the ARs promoted dust emission.

In the aforementioned studies, in-situ observations and reanalysis data sets at relatively coarse spatial resolution (no higher than 25 km) and temporal resolutions as low as once daily, are used to investigate the ARs and their impacts. Box et al. (2023) made use of a 2.5 km reanalysis product over Greenland to investigate extreme precipitation events in coastal regions, with daily totals in excess of 300 mm. They found linear, along-flow updraft regions embedded within the AR, termed "AR rapids," with a width of 5–15 km, 100–200 km long, and 3 km deep flowing about 2 km above sea level. AR rapids moved at high speed (>30 m s^{-1}), persisted for more than 24 hr, produced precipitation in their tracks, and were driven by buoyancy from condensation. Gravity waves triggered by the high-terrain further amplified the diabatic heating, increasing the rainfall rate by up to a factor of four. Such a complex structure will not be represented in coarse resolution modeling and observational products. However, if found to be ubiquitous in ARs, in particular in the more active ones, it may help explain their devastating impacts. It is important to stress that AR rapids are distinct from narrow cold-frontal rainbands, which exhibit a zig-zag or scalloped appearance in radar reflectivity and rain accumulation maps, are characterized by a "gap and core" structure with the bow-shaped core having a length of about 25–50 km, are coincident with and parallel to the cold front, and typically move at 10–20 m s^{-1} (Collins et al., 2020; Crosier et al., 2014; de Orla-Barile et al., 2022; Jorgensen et al., 2003). They are also distinct from mesoscale convective systems (MCSs; Nelli et al., 2021b), which are characterized by a broad area of deep convective clouds (>40,000 km^2) with a smaller precipitation region inside (>1,000 km^2), typically only lasting for a few hours (6–10 hr) and moving at lower speeds of 10–20 m s^{-1}. MCSs and AR rapids also leave contrasting imprints in the precipitation field, the former generating broader structures (Nelli et al., 2021b; da Silva and Haerter, 2023; Nelli, Francis, et al., 2021; Da Silva & Haerter, 2023) while the latter is characterized by linear streaks (Box et al., 2023). MCSs and AR rapids are therefore two different types of organized convection within an AR, with the former also existing outside ARs, for example, in association with convective outbreaks such as those that occur in the region in particular in the warmer months (Francis et al., 2021b).

The primarily goal of this study is to investigate AR rapids in mid-latitude regions such as the Middle East by scrutinizing the unusually strong AR of mid-April 2023, which caused widespread damage and loss of life in particular in Iraq (Al-Monitor, 2023) and Iran (Alarabiya News, 2023). This is achieved using a combination of observational, reanalysis data and a Weather Research and Forecasting (WRF; Skamarock et al., 2019) modeling

product. The findings of this work will help to further our current understanding of the dynamics of ARs and their interaction with other meteorological phenomena, and ultimately improve their prediction and contribute to minimizing their impacts.

The manuscript is structured as follows. The methods and data sets used in this work are summarized in Section 2. The large-scale dynamics that promoted the occurrence of the AR and its extreme nature are described in Section 3, with the mesoscale structure of the AR being discussed in Section 4, where the signatures of AR rapids are highlighted. The main findings of this study are outlined in Section 5.

2. Data Sets and Methodology

The large-scale processes that promoted the development of the AR are analyzed using ERA-5 reanalysis data (Hersbach et al., 2020), which has a spatial resolution of 0.25° (~27 km) and a temporal resolution of 1 hr. This state-of-the-art reanalysis data set has a good performance in the Middle East and North Africa in comparison with in-situ and satellite-derived measurements (Alghamdi, 2020; Fonseca et al., 2022b; Gleixner et al., 2020; Nogueira, 2020). ERA-5 is used to detect ARs using the same algorithm described in Guan and Waliser (2019), which employs a detection criteria based on intensity (above 85th percentile, or 100 kg m^{-1} s^{-1}, whichever is greater) and geometry (>2,000 km long, with a >2 length-to-width ratio) thresholds of IVT. This approach facilitates identifying ARs in traditionally IVT-low areas, helping to extend research into previously underexplored regions, such as that focused in the current study (Ma et al., 2021, 2024; Massoud et al., 2020; Wang et al., 2020; Zhang et al., 2023). It is one of the methods recommended by the Atmospheric River Tracking Method Intercomparison Project for application in dry regions (Rutz et al., 2019; Shields et al., 2018). Satellite images generated from the measurements collected by the Spinning Enhanced Visible and Infrared Imager (SEVIRI; Martinez et al., 2009; Schmetz et al., 2002) instrument onboard the Meteosat Second Generation spacecraft, available every 15-min at a resolution of 0.05° (~5.6 km), are used to visualize the associated cloud structure. Satellite-derived precipitation estimates from the Integrated Multi-Satellite Retrievals for the Global Precipitation Measurement (GPM) mission (IMERG; Huffman et al., 2020; Pradhan et al., 2022), available every 30-min at 0.1° (~11.1 km) resolution, and ground-based observations from weather stations that comprise the National Oceanic and Atmospheric Administration's Global Surface Summary of the Day (Lackey, 2020b) catalog, are used to assess the precipitation generated by the AR. In-situ hourly meteorological observations (Herzmann, 2024) and up to twice daily sounding profiles (Oolman, 2024) at airport stations are considered to inspect the local effects of the ARs. The moisture sources that contributed to the AR are identified through back-trajectories obtained with the Hybrid Single-Particle Lagrangian Integrated Trajectory (HYSPLIT; Stein et al., 2015) model driven by ERA-5 data.

In order to investigate the convection embedded within the AR and shed light on AR rapids, a numerical simulation is conducted with the WRF model, given the lack of high-resolution observational and reanalysis products for this region and time period. The WRF configuration used (Table S1) reflects the best set up for simulations of small-scale convective cells in the Arabian Peninsula (Fonseca et al., 2022a; Francis et al., 2021b; Gopalakrishnan et al., 2023; Taraphdar et al., 2021). The model is run in a 7.5–2.5 km nested configuration (Figure S1a in Supporting Information S1), with the innermost grid comprising the full Arabian Peninsula and having a spatial resolution that is high enough to resolve AR rapids (Box et al., 2023). An evaluation of the model predictions against ground-based and sounding data (Figure S1b in Supporting Information S1) revealed a good performance (Table S2 in Supporting Information S1).

3. Synoptic Dynamics and the Extreme Nature of the Atmospheric River

A dipole of pressure anomalies in the North Atlantic, projecting onto the positive phase of the North Atlantic Oscillation (NAO; Visbeck et al., 2001), a trough over southeastern Europe, and a ridge over India extending into the southeastern Arabian Peninsula are the main low-level large-scale circulation features over southern Europe, North Africa and the Middle East during 09–13 April 2023 (Figure 1a). The ridges over southwestern Europe and western Russia lead to a deflection of the polar jet, which converged with the subtropical jet over northeastern Africa (Figure 1b). The low over southeastern Europe is located to the north of the jet exit region, an area that is favorable for cyclogenesis (Wallace & Hobbs, 2006). This low, together with the ridge over India, Arabian Sea and Arabian Peninsula, led to a strong south-westerly flow in the Middle East, which fostered the development of the AR.

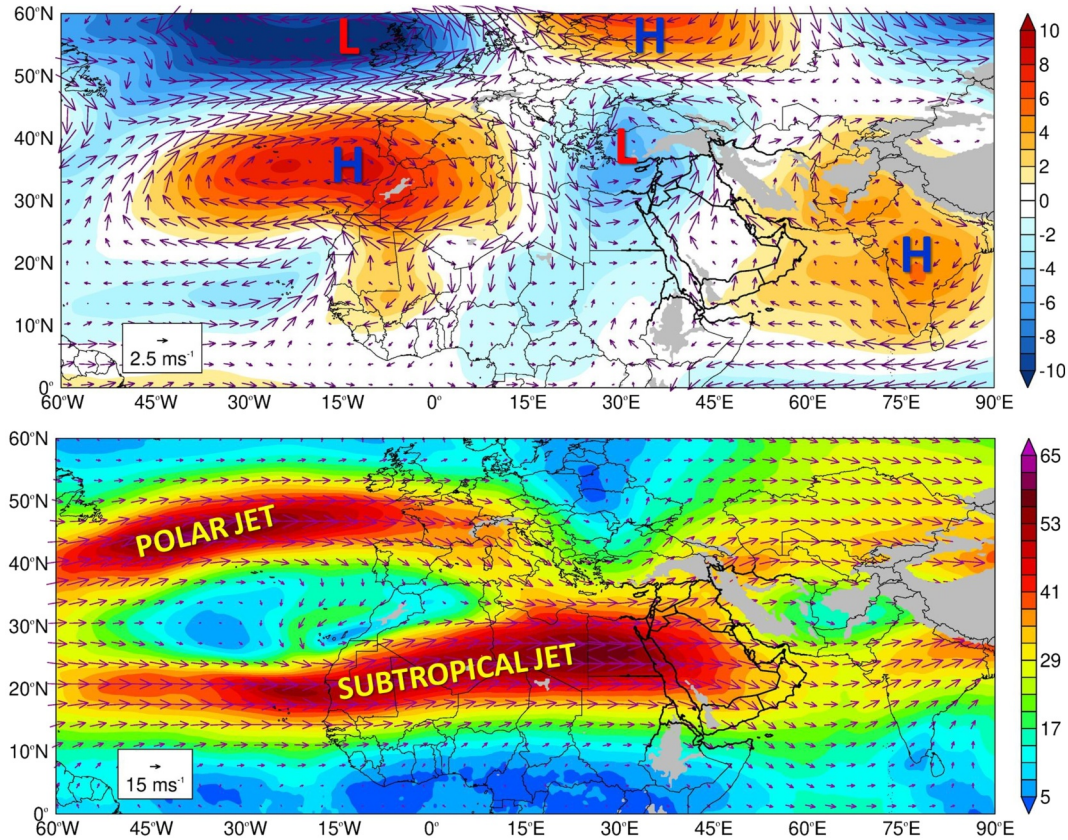

Figure 1. Synoptic atmospheric circulation averaged over 09–13 April 2023: (a) 850 hPa streamfunction (shading; 10^6 m^2 s^{-2}) and horizontal wind (arrows; m s^{-1}) anomalies. The major cyclonic and anticyclonic systems are highlighted with a red "L" and a blue "H," respectively. (b) 200 hPa horizontal wind speed (shading; m s^{-1}) and vectors (arrows). The position of the polar and subtropical jets are identified in the map. All fields are extracted from the ERA-5 reanalysis data, and are shown for the domain 60°W–60°E and 0°–60°N, with the anomalies computed with respect to the 1979–2022 3-hourly climatology.

Figure 2a shows the 500 hPa geopotential height and IVT on 11 April at 12 UTC, roughly 30 hr before the AR reached its peak intensity on 12 April at 18 UTC (Figure 2b). The AR on 12 April 2023 has a contribution from three moisture sources: (a) tropical Atlantic around 10°–20°N from the southwest; (b) North Atlantic and Mediterranean Sea from the northwest; (c) Red Sea, Gulf of Aden and Arabian Sea from the southeast and south. This is confirmed through back-trajectories (Figure S2 in Supporting Information S1). The maximum IVT associated with this AR was 1,176 kg m^{-1} s^{-1}, reached at 18 UTC on 12 April (Figure 2b), which makes it the strongest AR on record ahead of the 22 January 2005 AR (1,102 kg m^{-1} s^{-1}), reported to be the strongest AR in the Middle East in the 50-year period 1971–2020 (Esfandiari & Rezaei, 2022).

In order to further emphasize the extreme nature of this AR, Figure 2c shows a histogram of the 3rd spatial quartile of the hourly IVT in the Arabian Peninsula (10°–40°N and 30°–60°E) for the period 1979–2023, with the colored lines giving the minimum, mean and maximum values for 12 April 2023. The IVT values on 12 April are in the top 1% of the distribution, corresponding to a percentage of occurrence under 0.4%. The AR gradually strengthened during 11–12 April followed by a rapid weakening into 13 April, when the storm shifted eastwards and the AR moved over the Zagros mountains in Iran. As the moisture supply was cut off and the AR moved into high terrain and then further polewards, it quickly faded away. The presence of the Zagros mountains helped to spatially confine the moist air and led to the very high IVT values at 18 UTC on 12 April (Figure 2b).

4. Mesoscale Structure of the Atmospheric River—AR Rapids

Further insight into the dynamics of the AR is achieved through a high-resolution numerical simulation with the WRF model as detailed in Section 2. Figure 3a shows the observed and modeled near-surface fields at the location

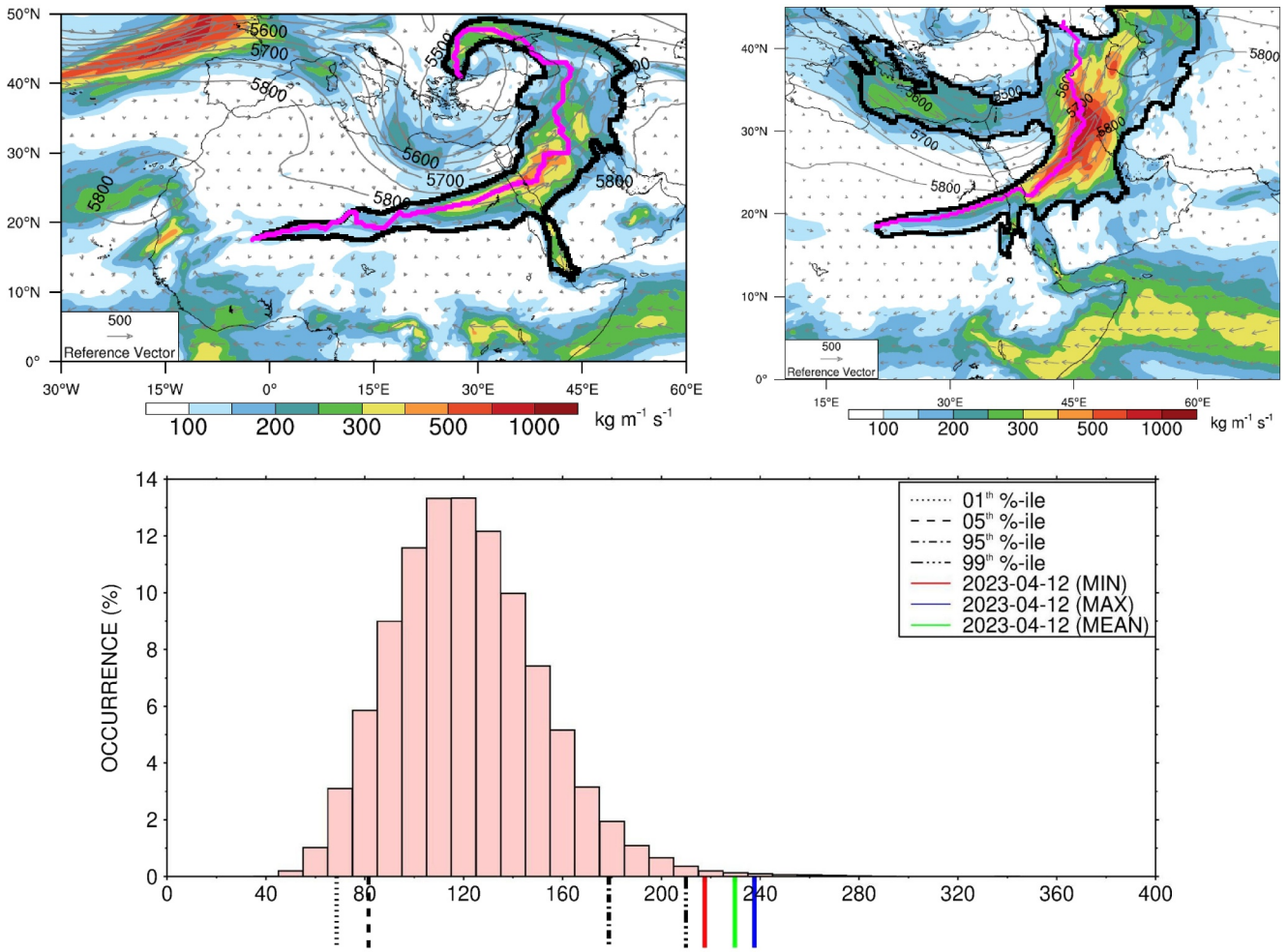

Figure 2. Atmospheric River during 11–13 April 2023: 500 hPa geopotential height (every 50 m; black contours) and Integrated Vapor Transport (IVT; the shading gives the magnitude and the arrows give the vectors; kg m^{-1} s^{-1}) on (a) 11 April at 12 UTC and (b) 12 April at 18 UTC from ERA-5. In (a) the fields are shown over 0°–50°N and 30°W–60°E, while (b) is a zoom-in map over the Middle East (0°–45°N, 10°E–70°E). The thick black line corresponds to the outline and extent of the AR while the thick purple line indicates the AR's axis where the IVT is strongest. (c) Histogram of the 3rd quartile of hourly IVT values in 10°–40°N and 30°–60°E from 1979 to 2023. The 1st, 5th, 95th and 99th percentiles are given the dotted, dashed, dash-dot and dash-dot-dot-dot black lines, respectively. The red, green and blue solid lines indicate the minimum, mean and maximum hourly values on 12 April 2023, respectively.

of the Baghdad International Airport (star in Figures 3b and 3c), a site that was directly affected by the AR and where its impacts were particularly severe (Al-Monitor, 2023).

The passage of the AR at 15 UTC on 11 April is characterized by a 12 K drop in air temperature, a 65% increase in relative humidity, a nearly tripling of the wind speed from 5 to 14 m s^{-1} with the wind direction shifting from southeast to west, and a 5 hPa variation in pressure in one hour, with the occurrence of rain and thunderstorms. This variability is more pronounced than that observed in a flood-producing AR in southwestern United States (Neiman et al., 2013), which is consistent with the extreme nature of this AR. The cold front associated with the mid-level trough moved over the site at 19 UTC on 13 April, when the skies cleared (Figure 3c), the wind direction shifted to the northwest, the relative humidity dropped by about 21%, and the air temperature decreased by roughly 4 K (Figure 3a). These changes are on the lower side of those reported in mid-latitude studies conducted in the northeastern Pacific (Norris et al., 2020) and Southern Ocean (Finlon et al., 2020; Rauber et al., 2020), probably due to the moderation of the cooler and drier air behind the cold front as it moved the warmer waters of the Mediterranean Sea and the northern Arabian Peninsula.

One way to gain further insight into the nature of the convection within the AR is through the isentropic streamfunction (Gopalakrishnan et al., 2023; Pauluis, 2016; Pauluis & Mrowiec, 2013). In Figures 3d and 3e, it

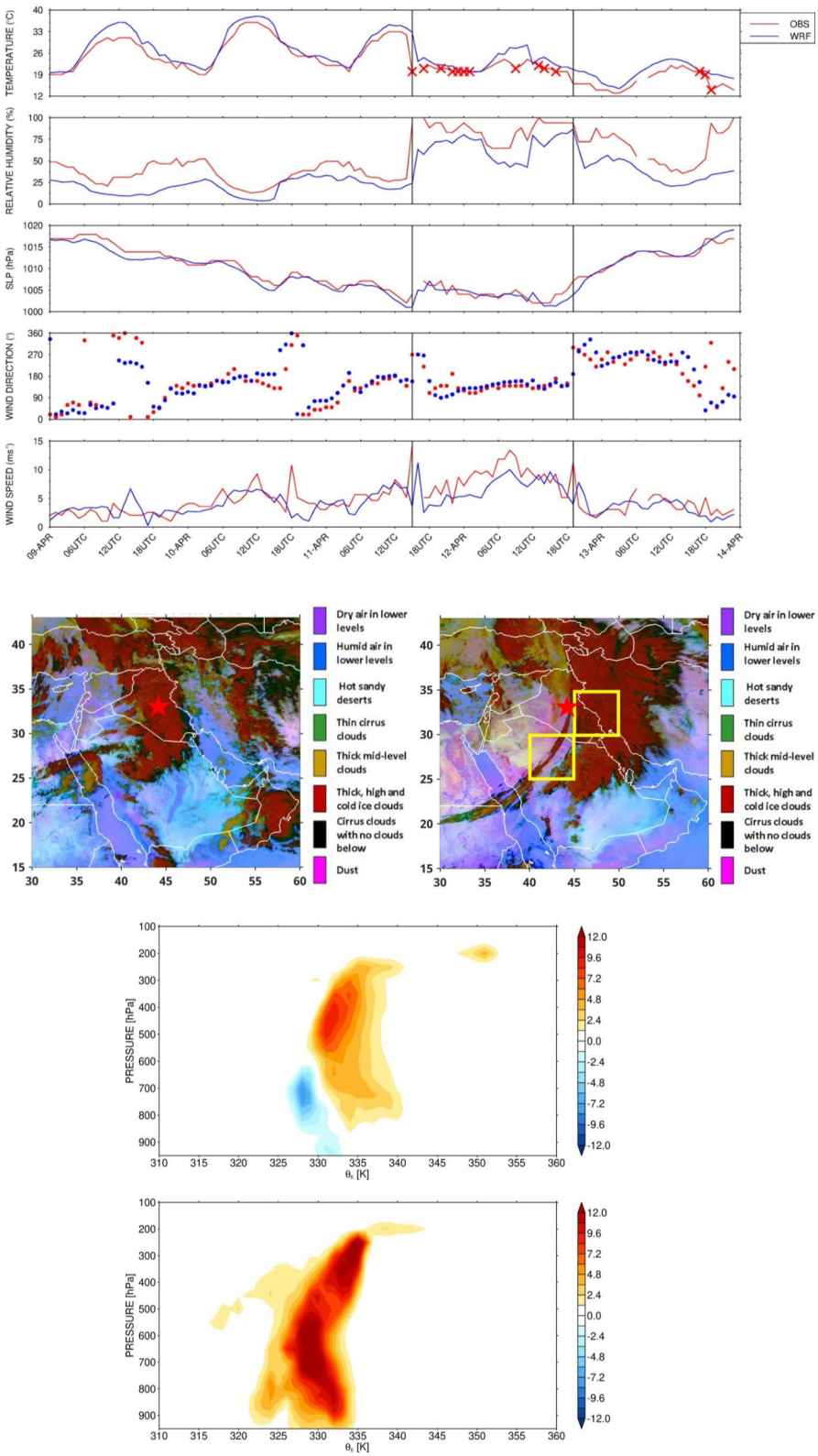

Figure 3.

is plotted for the domains highlighted by the yellow boxes in Figure 3c. In the local morning hours of 12 April, deep moist convection took place within the AR (note the maximum around 400–500 hPa at a θ_E of around 332.5 K) with convective downdrafts starting around 700 hPa and descending to the surface ($\theta_E \sim 327.5$ K). This is consistent with the observed convection in ARs (Finlon et al., 2020). The evening convection over eastern Iraq and western and southwestern Iran is very deep, with convective overshoots (i.e., strong updrafts above their level of neutral buoyancy) and the formation of extensive anvil clouds, and was associated with very high IVT values in excess of 1,100 kg m^{-1} s^{-1} (cf. Figure 2b). Compared to the morning convection, the updrafts in the evening convective event are not as energetic as the surface is colder (note the lower θ_E values), even though there is a reduced level of entrainment of the drier ambient air (compare the tilt of the updrafts in Figures 3d and 3e).

In order to explore the evolution of the convection in the AR, in Figures 4a and 4b the observed and WRF vertical profiles of equivalent potential temperature, relative humidity, and horizontal wind speed and direction at a station over northern Saudi Arabia (Figure S1b in Supporting Information S1) from 09 to 13 April are given. The model captures the major features such as the (a) jet streak at ∼200 hPa on 13 April with speeds in excess of 60 m s^{-1}, (b) shift of the wind from a southerly to a northerly direction on 11–12 April after the passage of the AR accompanied by a drying of the mid-troposphere, with a roughly ∼90% drop in relative humidity, and (c) drop in θ_E on 13–14 April, as drier and cooler air was advected into the site. These changes are consistent with those observed in the passage of the trailing cold front behind the AR (Finlon et al., 2020; Norris et al., 2020).

The 30-min WRF profiles are able to better resolve the features of the AR, including the presence of narrow but tall towers of high humidity on 10–12 April not seen in the 12-hr sounding profiles. These structures, called AR rapids, are roughly 2 km above the surface and extend up to the tropopause, propagating at high speed. The Hovmoeller plot in Figure 4c reveals they move at about 30 m s^{-1}, last at times for more than 24 hr, and generate copious amounts of precipitation in their wake, with rain rates in excess of 4 mm hr^{-1}. Their spatial and temporal scales match those of the AR rapids reported in Box et al. (2023), except that here they are deeper (5–7 vs. 3 km), in line with the fact that convection over southern Greenland is typically not as deep as in the Middle East. Vertical cross-sections confirm the presence of AR rapids (Figure S3 in Supporting Information S1), which are largely absent in ERA-5 data (Figure 4d) that just show broader regions of ascent. It is important to note that AR rapids are not present in satellite-derived products such as the SEVIRI images (Figures 3b and 3c), neither in the Infrared Brightness Temperature (Meyer, 2024) maps. Higher spatial (at least 2.5 km) and temporal (at least 30-min) frequency data are required to detect these features.

The Ha-il station is located downstream of the high-terrain in western Saudi Arabia (Figure S1b in Supporting Information S1), suggesting that gravity waves, seen in vertical cross-sections (Figures S3b and S3c in Supporting Information S1), may further increase the depth of the convection towers. Figure 4e gives the accumulated precipitation and maximum 10-m wind speed for 11–13 April. The wind speed field shows the signature of gravity waves, with peak values up to 35 m s^{-1}. The linear nature of the AR rapids seen in the Hovmoeller plot (Figure 4c) is also present in Figure 4e, and contrasts with the rainfall behind the mid-level trough, which shows a cyclonic curvature and is associated with the cooler and drier northwesterly air mass flowing over warmer sea surface temperatures. A similar spatial pattern is present in the satellite-derived GPM IMERG estimates (Figure S4a in Supporting Information S1). The 3-day accumulated rainfall exceeds 200 mm over the high-terrain, with peak values just over 450 mm. The peak value in the ∼11 km satellite product is roughly half of that predicted by WRF's 2.5 km grid, ∼210 mm, and is largely comparable to the ∼240 mm predicted by WRF's 7.5 km grid. This suggests the increased rainfall amounts in the finer nest may arise from a more detailed representation of the complex topography of the Zagros Mountains. There

Figure 3. Convection within the Atmospheric River: (a) Observed (red) and WRF (blue) hourly air temperature (°C), relative humidity (%), sea-level pressure (hPa) and horizontal wind direction (°), and speed (m s^{-1}) at the Baghdad International Airport, station #30 in Figure S1b in Supporting Information S1 and star in panels (b) and (c), from 09 to 13 April 2023. Times when precipitation and/or thunderstorms occurred at the site are highlighted with crosses in the top panel. SEVIRI false-color satellite images on (b) 11 April at 15 UTC, and (c) 12 April at 19 UTC, the times highlighted with a vertical line in panel (a). Isentropic streamfunction (10^{-3} kg m^{-2} s^{-1}) on (d) 12 April averaged over 25°–30°N and 40°–45°E, bottom yellow box in panel (c), and 04–09 UTC, and (e) 30°–35°N and 45°–50°E, upper yellow box in panel (c), and 18–23 UTC.

10.1029/2024GL109446

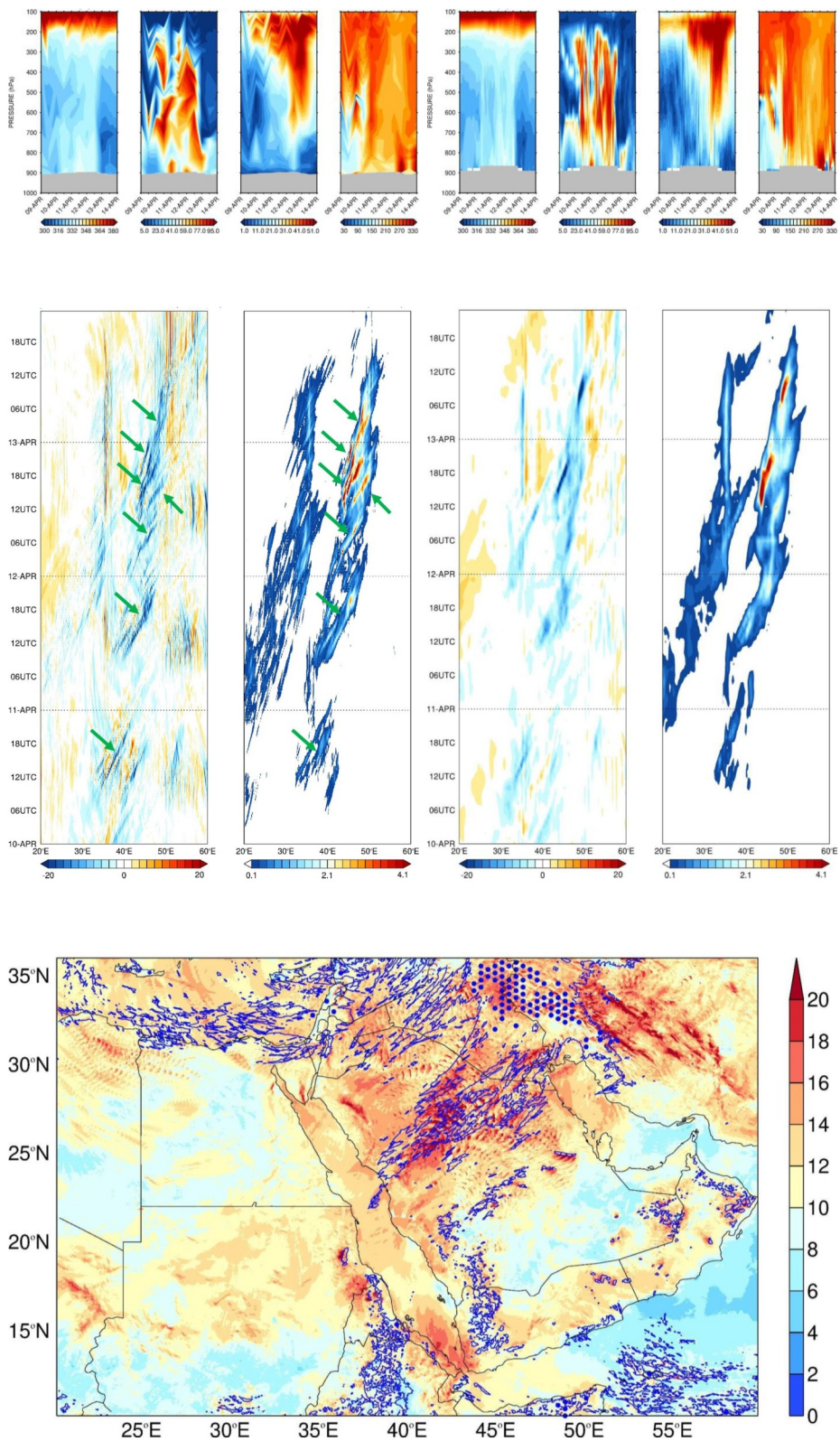

Figure 4.

are very few weather stations in this region, and even fewer with full precipitation records from 11 to 13 April 2023. The highest accumulated rainfall is ∼120 mm for a station in northern Iraq (Figure S4b in Supporting Information S1), for which the WRF's 2.5 km grid (∼94 mm) and GPM IMERG (∼92 mm) estimates are not too far off.

5. Discussion and Conclusions

ARs can deliver life-threatening amounts of rainfall in mid- and high-latitudes, even though the precipitation can be beneficial in drier subtropical regions and during drought periods (Lamjiri et al., 2017). Despite the extensive research conducted on this topic, and owing to the sparse observational measurements and the still low spatial resolution modeling and reanalysis data sets, very few studies have delved into the finer structure of the convection within an AR such as AR rapids. In this study, the anatomy and dynamics of one of the strongest AR to impact the Middle East in mid-April 2023 that wreaked havoc leading to extensive damage and multiple deaths in particular in Iraq and Iran, is investigated. This is achieved using a combination of observations and reanalysis data and a nested model simulation.

The presence of a ridge over India extending into the southeastern Arabian Peninsula and a trough over southeastern Europe promoted the development of the AR. Both tropical and extratropical moisture sources contributed to the exceptionally-high IVT values. The third quartile of the IVT in the Arabian Peninsula is in the top 1% of the climatological distribution, with a maximum IVT of 1,176 kg m^{-1} s^{-1}. Ground-based observations and radiosonde profiles exhibit the classic signatures of AR conditions and the passage of the cold front behind the AR, which are generally well simulated by the numerical model. The 30-min vertical profiles revealed the presence of AR rapid-like structures, composed of convective cells with similar characteristics to those reported by Box et al. (2023), albeit deeper in the vertical (5–7 vs. 3 km), as the environment in the Middle East is more conducive for convection. Such features are not explicitly present in the ∼27 km resolution ERA-5 data.

The findings of this research pave the way for new research and investigation avenues. Moving forward, future work can build upon these results to delve deeper into the dynamics behind ARs, in particular of its multi-scale nature and the interaction between larger-scale convection and smaller-scale features such as AR rapids, their seasonality and variability. It will also be of interest to investigate whether AR rapid-like structures are present in all ARs or just in specific ones, whether their main features (length, width, depth, propagation speed and duration) vary from one AR to another, and where and at what stage of the AR they are more likely to occur. These questions can be addressed through the analysis of a reanalysis product at 2.5 km resolution or higher, or through the modeling of a large number of individual events.

The circulation patterns that promote ARs comprising AR rapid-like structures should also be investigated. Once a basic understanding is gained, the focus should be on multi-scale interactions, for which observations collected during dedicated field campaigns will be crucial. Feature extraction and tracking techniques, spectral analysis and regression and composites (Fonseca et al., 2019; van der Linden et al., 2016) are some of the methodologies that can be considered. The potential role of the low- and high-level jets on AR rapids development are also worth exploring. Ultimately, the development of an index or scale for AR rapids will be vital for operational purposes, and help in mitigating their potential devastating impacts. As ARs are projected to become more frequent and intense in a warming climate (Payne et al., 2020; Shields et al., 2023; Wang et al., 2023), including in the Middle East (Espinoza et al., 2018; Massoud et al., 2019), understanding their dynamics in the present climate will contribute to a better comprehension of their projected changes in the future.

Figure 4. Atmospheric River Rapids: (a) Equivalent potential temperature (θ_E; K), relative humidity (%) and horizontal wind speed (m s^{-1}) and direction (°) from radiosondes launched at the Ha-Il Regional Airport (station #6 in Figure S1b in Supporting Information S1) every 12-hr from 09 to 13 April 2023. Panel (b) is as (a) but with the 30-min WRF output. (c) Hovmoeller plot of the WRF model's 30-min 600 hPa vertical velocity (10^{-2} m s^{-1}) and precipitation rate (mm hr^{-1}) averaged over 30°–35°N from 09–13 April 2023. The AR rapids are highlighted by the green arrows. Panel (d) is as (c) but with the hourly ERA-5 data. (e) Maximum 10-m wind speed (m s^{-1}; shading) and accumulated precipitation (10 mm contour plotted as a solid blue line; blue dots indicate regions where it exceeds 50 mm) for 11–13 April from WRF. Satellite-derived and in-situ measured precipitation amounts for the same period are given in Figure S4 in Supporting Information S1.

Conflict of Interest

The authors declare no conflicts of interest relevant to this study.

Data Availability Statement

The data used to generate all the figures in this manuscript is available online at Francis et al. (2024; https://doi.org/10.5281/zenodo.10634350). The observational and reanalysis products considered in this study are freely available online. ERA-5 reanalysis data, available at ∼27 km spatial resolution and hourly temporal resolution, is extracted from the Copernicus Climate Data Store's website (Hersbach et al., 2024a, 2024b). Sounding profiles available at best twice daily are downloaded from the University of Wyoming's website (Oolman, 2024) while ground-based hourly observations at airport stations, Meteorological Aerodrome Reports, are freely available at the Iowa State University Iowa Environmental Mesonet's website (Herzmann, 2024). The National Oceanic and Atmospheric Administration (NOAA) Global Surface Summary of the Day (GSOD) data is downloaded from the NOAA's National Centers for Environmental Information website (Lackey, 2020a). The Spinning Enhanced Visible and Infrared Imager (SEVIRI) images are extracted from The European Organisation for the Exploitation of Meteorological Satellites website (EUMETSAT, 2024), while the satellite-derived Infrared Brightness Temperature, at 4 km spatial and 30-min temporal resolution, is downloaded from the National Aeronautic and Space Administration's Earthdata website (Meyer, 2024). The Integrated Multi-Satellite Retrievals for the Global Precipitation Measurement (GPM) mission (IMERG) is extracted from the National Aeronautic and Space Administration's Goddard Earth Sciences Data and Information Services Center website (Huffman et al., 2019). The WRF model used in this work is version 4.3.3, and is freely available from the developers' website (WRF, 2023). The authors gratefully acknowledge the National Oceanic and Atmospheric Administration (NOAA) Air Resources Laboratory for the provision of the Hybrid Single-Particle Lagrangian Integrated Trajectory (HYSPLIT) transport and dispersion model (NOAA ARL, 2024).

Acknowledgments

The authors wish to acknowledge the contribution of Khalifa University's high-performance computing and research computing facilities to the results of this research. We also gratefully acknowledge the National Oceanic and Atmospheric Administration (NOAA) Air Resources Laboratory (ARL) for the provision of the HYSPLIT transport and dispersion model through the Real-time Environmental Applications and Display System (READY) website (https://www.ready.noaa.gov/) used in this publication. We would like to thank the editor and two anonymous reviewers for their several constructive and insightful comments and suggestions that have led to a substantial improvement of the quality of this work. This work was supported by Khalifa University through Grant number 8474000641.

References

Alarabiya News. (2023). Heavy rains in Iran trigger flash floods, killing at least two. Retrieved from https://english.alarabiya.net/News/middle-east/2023/04/13/Heavy-rains-in-Iran-trigger-flash-floods-killing-at-least-two

Alghamdi, A. S. (2020). Evaluation of four reanalysis datasets against radiosonde over southwest Asia. *Atmosphere*, *11*(4), 402. https://doi.org/10.3390/atmos11040402

Alghamdi, A. S., & Harrington, J., Jr. (2022). Spatiotemporal climatology of the Arabian subtropical anticyclone. *Physical Geography*, *43*(5), 659–679. https://doi.org/10.1080/02723646.2022.2080902

Alghamdi, A. S., & Harrington, J., Jr. (2023). The symmetry and structural characteristics of the core of the Arabian subtropical anticyclone and associated surface climatology over Arabia: A spatial perspective. *Atmospheric Research*, *281*, 106482. https://doi.org/10.1016/j.atmosres.2022.106482

Al-Monitor. (2023). Severe floods in Iraq leave several dead, adding to climate strains. Retrieved from https://www.al-monitor.com/originals/2023/04/severe-floods-iraq-leave-several-dead-adding-climate-strains

Box, J. E., Nielsen, K. P., Yang, X., Niwano, M., Wehrie, A., van As, D., et al. (2023). Greenland ice sheet rainfall climatology, extremes and atmospheric river rapids. *Meteorological Applications*, *30*(4), e2134. https://doi.org/10.1002/met.2134

Bozkurt, D., Sen, O. L., Ezber, Y., Guan, B., Viale, M., & Caglar, F. (2021). Influence of African atmospheric rivers on precipitation and snowmelt in the Near East's highlands. *Journal of Geophysical Research: Atmospheres*, *126*(4), e2020JD033646. https://doi.org/10.1029/2020JD033646

Chakraborty, S., Guan, B., Waliser, D. E., & da Silva, A. M. (2022). Aerosol atmospheric rivers: Climatology, event characteristics, and detection algorithm sensitivities. *Atmospheric Chemistry and Physics*, *22*(12), 8175–8195. https://doi.org/10.5194/acp-22-8175-2022

Chakraborty, S., Guan, B., Waliser, D. E., da Silva, A. M., Uluatam, S., & Hess, P. (2021). Extending the atmospheric river concept to aerosols: Climate and air quality impacts. *Geophysical Research Letters*, *48*(9), e2020GL091827. https://doi.org/10.1029/2020GL091827

Collins, B. D., Oakley, N. S., Perkins, J. P., East, A. E., Corbett, S. C., & Hatchett, B. J. (2020). Linking mesoscale meteorology with extreme landscape response: Effects of narrow cold frontal rainbands (NCFRs). *Journal of Geophysical Research: Earth Surface*, *125*(10), e2020JF005675. https://doi.org/10.1029/2020JF005675

Crosier, J., Choularton, T. W., Westbrook, C. D., Blyth, A. M., Bower, K. N., Connolly, P. J., et al. (2014). Microphysical properties of cold frontal rainbands. *Quarterly Journal of the Royal Meteorological Society*, *140*(681), 1257–1268. https://doi.org/10.1002/qj.2206

Da Silva, N. A., & Haerter, J. O. (2023). The precipitation characteristics of mesoscale convective systems over Europe. *Journal of Geophysical Research: Atmospheres*, *128*(23), e2023JD039045. https://doi.org/10.1029/2023JD039045

de Orla-Barile, M., Cannon, F., Oakley, N. S., & Ralph, F. M. (2022). A climatology of narrow cold-fronal rainbands in Southern California. *Geophysical Research Letters*, *49*(2), e2021GL095362. https://doi.org/10.1029/2021GL095362

de Vries, A. J., Feldstein, S. B., Riemer, M., Tyrlis, E., Sprenger, M., Baumgart, M., et al. (2016). Dynamics of tropical-extratropical interactions and extreme precipitation events in Saudi Arabia in autumn, winter and spring. *Quarterly Journal of the Royal Meteorological Society*, *142*(697), 1862–1880. https://doi.org/10.1002/qj.2781

de Vries, A. J., Tyrlis, E., Edry, D., Krichak, S. O., Steil, B., & Lelieveld, J. (2013). Extreme precipitation events in the Middle East: Dynamics of the active Red Sea Trough. *Journal of Geophysical Research: Atmospheres*, *118*(13), 7087–7108. https://doi.org/10.1002/jgrd.50569

Dezfuli, A. (2020). Rare Atmospheric River caused record floods across the Middle East. *Bulletin of the American Meteorological Society*, *101*(4), E394–E400. https://doi.org/10.1175/BAMS-D-19-0247.1

Dezfuli, A., Bosilovich, M. G., & Barahona, D. (2021). A dusty atmospheric river brings floods to the Middle East. *Geophysical Research Letters*, *48*(23), e2021GL095441. https://doi.org/10.1029/202GL095441

Eiras-Barca, J., Ramos, A. M., Algarra, I., Vazquez, M., Dominguez, F., Miguez-Macho, G., et al. (2021). European west coast atmospheric rivers: A scale to characterize strength and impacts. *Weather and Climate Extremes*, *31*, 100305. https://doi.org/10.1016/j.wace.2021.100305

Esfandiari, N., & Lashkari, H. (2020). Identifying atmospheric river events and their paths into Iran. *Theoretical and Applied Climatology*, *140*(3–4), 1125–1137. https://doi.org/10.1007/s00704-020-03148-w

Esfandiari, N., & Rezaei, M. (2022). Automatic detection, classification, and long-term investigation of temporal-spatial changes of atmospheric rivers in the Middle East. *International Journal of Climatology*, *42*(15), 7730–7750. https://doi.org/10.1002/joc.7674

Espinoza, V., Waliser, D. E., Guan, B., Lavers, D. A., & Ralph, F. M. (2018). Global analysis of climate change projection effects on atmospheric rivers. *Geophysical Research Letters*, *45*(9), 4299–4308. https://doi.org/10.1029/2017GL076968

EUMETSAT. (2024). Earth observational portal [Dataset]. *European Organisation for the Exploitation of Meteorological Satellites*. Retrieved from https://eoportal.eumetsat.int

Finlon, J. A., Rauber, R. M., Wu, W., Zaremba, T. J., McFarquhar, G. M., Nesbitt, S. W., et al. (2020). Structure of an Atmospheric River over Australia and the Southern Ocean: II. Microphysical evolution. *Journal of Geophysical Research: Atmospheres*, *125*(18), e2020JD032514. https://doi.org/10.1029/2020JD032514

Flaounas, E., Davolio, S., Raveh-Rubin, S., Pantillon, F., Miglietta, M. M., Gaertner, M. A., et al. (2022). Mediterranean cyclones: Current knowledge and open questions on dynamics, prediction, climatology and impacts. *Weather and Climate Dynamics*, *3*(1), 173–208. https://doi.org/10.5194/wcd-3-173-2022

Fonseca, R., Francis, D., Aulicino, G., Mattingly, K. S., Fusco, G., & Budillon, G. (2023). Atmospheric controls on the Terra Nova Bay polynya occurrence in Antarctica. *Climate Dynamics*, *61*(11–12), 5147–5169. https://doi.org/10.1007/s00382-023-06845-0

Fonseca, R., Francis, D., Nelli, N., Farrah, S., Wehbe, Y., Al Hosari, T., & Al Mazroui, A. (2022a). Assessment of the WRF model as a guidance tool into cloud seeding operations in the United Arab Emirates. *Earth and Space Science*, *9*(5), e2022EA002269. https://doi.org/10.1029/2022EA002269

Fonseca, R., Francis, D., Nelli, N., & Thota, M. (2022b). Climatology of the heat low and the intertropical discontinuity in the Arabian Peninsula. *International Journal of Climatology*, *42*(2), 1092–1117. https://doi.org/10.1002/joc.7291

Fonseca, R., Koh, T.-Y., & Teo, C.-K. (2019). Multi-scale interactions in a high-resolution tropical-belt experiment and observations. *Climate Dynamics*, *52*(5–6), 3503–3532. https://doi.org/10.1007/s00382-018-4332-y

Francis, D., Fonseca, R., Mattingly, K. S., Marsh, O. J., Lhermitte, S., & Cherif, C. (2022a). Atmospheric triggers of the brunt ice shelf calving in February 2021. *Journal of Geophysical Research: Atmospheres*, *127*(11), e2021JD036424. https://doi.org/10.1029/2021JD036424

Francis, D., Fonseca, R., Nelli, N., Bozkurt, D., & Guan, B. (2024). Role of atmospheric river rapids in the April 2023 middle east flash floods [Dataset]. *Zenodo*. https://doi.org/10.5281/zenodo.10634350

Francis, D., Fonseca, R., Nelli, N., Bozkurt, D., Picard, G., & Guan, B. (2022b). Atmospheric rivers drive exceptional Saharan dust transport towards Europe. *Atmospheric Research*, *266*, 105959. https://doi.org/10.1016/j.atmosres.2021.105959

Francis, D., Fonseca, R., Nelli, N., Bozkurt, D., Picard, G., & Guan, B. (2023). On the Middle East's severe dust storms in spring 2022: Triggers and impacts. *Atmospheric Environment*, *296*, 119539. https://doi.org/10.1016/j.atmosenv.2022.119539

Francis, D., Mattingly, K. S., Lhermitte, S., Temimi, M., & Heil, P. (2021a). Atmospheric extremes caused high oceanward sea surface slope triggering the biggest calving event in more than 50 years at the Amery Ice Shelf. *The Cryosphere*, *15*(5), 2147–2165. https://doi.org/10.5194/tc-15-2147-2021

Francis, D., Mattingly, K. S., Temimi, M., Massom, R., & Heil, P. (2020). On the crucial role of atmospheric rivers in the two major Weddell Polynya events in 1973 and 2017 in Antarctica. *Science Advances*, *6*(46). https://doi.org/10.1126/sciadv.abc2695

Francis, D., Temimi, M., Fonseca, R., Nelli, N. R., Abida, R., Weston, M., & Whebe, Y. (2021b). On the analysis of a summertime convective event in a hyperarid environment. *Quarterly Journal of the Royal Meteorological Society*, *147*(734), 501–525. https://doi.org/10.1002/qj.3930

Gimeno, L., Nieto, R., Vazquez, M., & Lavers, D. A. (2014). Atmospheric rivers: A mini-review. *Frontiers in Earth Science*, *2*. https://doi.org/10.3389/feart.2014.00002

Gleixner, S., Demissie, T., & Diro, G. T. (2020). Did ERA5 improve temperature and precipitation reanalysis over east Africa? *Atmosphere*, *11*(9), 996. https://doi.org/10.3390/atmos11090996

Gopalakrishnan, D., Taraphdar, S., Pauluis, O. M., Xue, L., Ajayamohan, R. S., Al Shamsi, N., et al. (2023). Anatomy of a summertime convective event over the Arabian region. *Monthly Weather Review*, *151*(4), 989–1004. https://doi.org/10.1175/MWR-D-22-0082.1

Guan, B., & Waliser, D. E. (2015). Detection of atmospheric rivers: Evaluation and application of an algorithm for global studies. *Journal of Geophysical Research: Atmospheres*, *120*(24), 12514–12535. https://doi.org/10.1002/2015JD02457

Guan, B., & Waliser, D. E. (2019). Tracking atmospheric rivers globally: Spatial distributions and temporal evolution of life cycle characteristics. *Journal of Geophysical Research: Atmospheres*, *124*(23), 12523–12552. https://doi.org/10.1029/2019JD031205

Guan, B., Waliser, D. E., & Ralph, F. M. (2023). Global application of the atmospheric river scale. *Journal of Geophysical Research: Atmospheres*, *128*(3), e2022JD037180. https://doi.org/10.1029/2022JD037180

Hersbach, H., Bell, B., Berrisford, P., Biavati, G., Horanyi, A., Munoz Sabater, J., et al. (2024a). ERA5 hourly data on single levels from 1940 to present [Dataset]. *Copernicus Climate Change Service Climate Data Store*. https://doi.org/10.24381/cds.adbb2d47

Hersbach, H., Bell, B., Berrisford, P., Biavati, G., Horanyi, A., Munoz Sabater, J., et al. (2024b). ERA5 hourly data on pressure levels from 1940 to present [Dataset]. *Copernicus Climate Change Service Climate Data Store*. https://doi.org/10.24381/cds.bd0915c6

Hersbach, H., Bell, B., Berrisford, P., Hirahara, S., Horanyi, A., Munoz-Sabater, J., et al. (2020). The ERA5 global reanalysis. *Quarterly Journal of the Royal Meteorological Society*, *146*(730), 1999–2049. https://doi.org/10.1002/qj.3803

Herzmann, D. (2024). Iowa environmental mesonet [Dataset]. *Iowa State University*. https://mesonet.agron.iastate.edu/request/download.phtml

Huffman, G. J., Bolvin, D. T., Braithwaite, D., Hsu, K.-L., Joyce, R. J., Kidd, C., et al. (2020). Integrated multi-satellite retrievals for the global precipitation measurement (GPM) mission (IMERG). In V. Levizzani, C. Kidd, D. B. Kirschbaum, C. D. Kummerow, K. Nakamura, & F. J. Turk (Eds.), *Satellite precipitation measurement*, *Advances in global change research* (Vol. 67, pp. 343–353). Springer. https://doi.org/10.1007/978-3-030-24568-9_19

Huffman, G. J., Stocker, E. F., Bolvin, D. T., Nelkin, E. J., & Tan, J. (2019). GPM IMERG early precipitation L3 1 day 0.1 degree x 0.1 degree V07 [Dataset]. *Goddard Earth Sciences Data and Information Services Center*. https://doi.org/10.5067/GPM/IMERGDF/DAY/07

Jorgensen, D. P., Pu, Z., Persson, P. O. G., & Tao, W.-K. (2003). Variations associated with cores and gaps of a Pacific narrow cold frontal rainband. *Monthly Weather Review*, *131*(11), 2705–2729. https://doi.org/10.1175/1520-0493(2003)131<2705:VAWCAG>2.0.CO;2

Lackey, M. (2020a). Global surface summary of the day [Dataset]. *National Oceanic and Atmospheric Administration National Centers for Environmental Information*. https://www.ncei.noaa.gov/access/metadata/landing-page/bin/iso?id=gov.noaa.ncdc:C00516

Lackey, M. (2020b). Special notes on the national centers for environmental information global surface summary of the day data. Retrieved from https://www.ncei.noaa.gov/data/global-summary-of-the-day/doc/readme.txt

Lamjiri, M. A., Dettinger, M. D., Ralph, F. M., & Guan, B. (2017). Hourly storm characteristics along the U.S. West Coast: Role of atmospheric rivers in extreme precipitation. *Geophysical Research Letters*, *44*(13), 7020–7028. https://doi.org/10.1002/2017GL074193

Lapere, R., Tomas, J. L., Favier, V., Angot, H., Asplund, J., Ekman, A. M. L., et al. (2024). Polar aerosol atmospheric rivers: Detection, characteristics, and potential applications. *Journal of Geophysical Research: Atmospheres*, *129*(2), e2023JD039606. https://doi.org/10.1029/2023JD039606

Lavers, D. A., & Villarini, G. (2015). The contribution of atmospheric rivers to precipitation in Europe and the United States. *Journal of Hydrology*, *522*, 382–390. https://doi.org/10.1016/j.hydrol.2014.12.010

Liang, J., & Yong, Y. (2021). Climatology of atmospheric rivers in the Asian monsoon region. *International Journal of Climatology*, *41*(S1), E801–E818. https://doi.org/10.1002/joc.6729

Lionello, P., Trigo, I. F., Gil, V., Liberato, M. L. R., Miessen, K. M., Pinto, J. G., et al. (2016). Objective climatology of cyclones in the Mediterranean region: A consensus view among methods with different system identification and tracking criteria. *Tellus A: Dynamic Meteorology and Oceanography*, *68*(1), 29391. https://doi.org/10.3402/tellusa.v68.29391

Lora, J. M., Shields, C. A., & Rutz, J. J. (2020). Consensus and disagreement in atmospheric river detection: ARTMIP global catalogues. *Geophysical Research Letters*, *47*(20), e2020GL089302. https://doi.org/10.1029/2020GL089302

Ma, W., Chen, G., Peings, Y., & Alviz, N. (2021). Atmospheric river response to arctic sea ice loss in the polar amplification model intercomparison project. *Geophysical Research Letters*, *48*(20), e2021GL094883. https://doi.org/10.1029/2021GL094883

Ma, W., Wang, H., Chen, G., Leung, L. R., Lu, J., Rasch, P. J., et al. (2024). The role of interdecadal climate oscillations in driving Arctic atmospheric river trends. *Nature Communications*, *15*(1), 2135. https://doi.org/10.1038/s41467-024-45159-5

Martinez, M. A., Ruiz, J., & Cuevas, E. (2009). Use of SEVIRI images and derived products in a WMO sand and dust storm warning system. *IOP Conference Series: Earth and Environmental Science*, *7*, 012004. https://doi.org/10.1088/1755-1307/7/1/012004

Massoud, E., Massoud, T., Guan, B., Sengupta, A., Espinoza, V., De Luna, M., et al. (2020). Atmospheric rivers and precipitation in the middle east and north America (MENA). *Water*, *12*(10), 2863. https://doi.org/10.3390/w12102863

Massoud, E. C., Espinoza, V., Guan, B., & Waliser, D. E. (2019). Global climate model ensemble approaches for future projections of atmospheric rivers. *Earth's Future*, *7*(10), 1136–1151. https://doi.org/10.1029/2019EF001249

Meinander, O., Kouznetsov, R., Uppstu, A., Sofiev, M., Kaakinen, A., Salminen, J., et al. (2023). African dust transport and deposition modeling verified through a citizen science campaign in Finland. *Scientific Reports*, *13*(1), 21379. https://doi.org/10.1038/s41598-023-46321-7

Meyer, D. (2024). NCEP/CPC L3 half hourly 4km global (60S - 60N) merged IR V1 (GPM_MERGIR) [Dataset]. *National Centers for Environmental Prediction/Climate Prediction Center*. https://disc.gsfc.nasa.gov/datasets/GPM_MERGIR_1/summary

Neiman, P. J., Ralph, F. M., Moore, B. J., Hughes, M., Mahoney, K. M., Cordeira, J. M., & Dettinger, M. D. (2013). The landfall and inland penetration of flood-producing atmospheric river in Arizona. Part I: Observed synoptic-scale, orographic, and hydrometeorological characteristics. *Journal of Hydrometeorology*, *14*(2), 460–484. https://doi.org/10.1175/JHM-D-12-0101.1

Nelli, N., Fissehaye, S., Francis, D., Fonseca, R., Temimi, M., Weston, M., et al. (2021a). Characteristics of atmospheric aerosols over the UAE inferred from CALIPSO and sun photometer aerosol optical depth. *Earth and Space Science*, *8*(6), e2020EA001360. https://doi.org/10.1029/2020EA001360

Nelli, N. R., Francis, D., Fonseca, R., Abida, R., Weston, M., Wehbe, Y., & Al Hosary, T. (2021b). The atmospheric controls of extreme convective events over the southern Arabian Peninsula during the spring season. *Atmospheric Research*, *262*, 105788. https://doi.org/10.1016/j.atmosres.2021.105788

Nellikkattil, A. B., Lee, J. Y., Guan, B., Timmermann, A., Lee, S.-S., Chu, J.-E., & Lemmon, D. (2023). Increased amplitude of atmospheric rivers and associated extreme precipitation in ultra-high-resolution greenhouse warming simulations. *Communications Earth & Environment*, *4*(1), 313. https://doi.org/10.1038/s43247-023-00963-7

NOAA ARL. (2024). HYSPLIT for Linux - Public (unregistered) version download [Software]. *National Oceanic and Atmospheric Administration Air Resources Laboratory*. Retrieved from https://www.ready.noaa.gov/HYSPLIT_linuxtrial.php

Nogueira, M. (2020). Inter-comparison of ERA-5, ERA-Interim and GPCP rainfall over the last 40 years: Process-based analysis of systematic and random differences. *Journal of Hydrology*, *583*, 124632. https://doi.org/10.1016/j.jhydrol.2020.124632

Norris, J. R., Ralph, F. M., Demirdjian, R., Cannon, F., Blomquist, B., Fairall, C. W., et al. (2020). The observed water vapor budget in an atmospheric River over the Northeast Pacific. *Journal of Hydrometeorology*, *21*(11), 2655–2673. https://doi.org/10.1175/JHM-D-20-0048.1

Oolman, L. (2024). Atmospheric soundings [Dataset]. *University of Wyoming*. https://weather.uwyo.edu/upperair/sounding.html

Park, C., Son, S.-W., & Guan, B. (2023). Multiscale nature of atmospheric rivers. *Geophysical Research Letters*, *50*(10), e2023GL102784. https://doi.org/10.1029/2023GL102784

Park, C., Son, S.-W., & Kim, H. (2021). Distinct features of atmospheric rivers in the early versus late East Asian summer monsoon and their impacts on monsoon rainfall. *Journal of Geophysical Research: Atmospheres*, *126*(7), e2020JD033537. https://doi.org/10.1029/2020JD033537

Pauluis, O. M. (2016). The mean air flow as Lagrangian dynamics approximation and its application to moist convection. *Journal of the Atmospheric Sciences*, *73*(11), 4407–4425. https://doi.org/10.1175/JAS-D-15-0284.1

Pauluis, O. M., & Mrowiec, A. A. (2013). Isentropic Analysis of convective motions. *Journal of the Atmospheric Sciences*, *70*(11), 3673–3688. https://doi.org/10.1175/JAS-D-12-0205.1

Payne, A. E., Demory, M.-E., Leung, L. R., Ramos, A. M., Shields, C. A., Rutz, J. J., et al. (2020). Responses and impacts of atmospheric rivers to climate change. *Nature Reviews Earth & Environment*, *1*(3), 143–157. https://doi.org/10.1038/s43017-020-0030-5

Pradhan, R. K., Markonis, Y., Godoy, M. R. V., Villalba-Pradas, A., Andreadis, K. M., Nikolopoulos, E. I., et al. (2022). Review of GPM IMERG performance: A global perspective. *Remote Sensing of Environment*, *268*, 112754. https://doi.org/10.1016/j.rse.2021.112754

Ralph, F., Smallcomb, C. M., Rutz, J. J., Cordeira, J. M., Dettinger, M., Anderson, M., & Reynolds, D. (2019). A scale to characterize the strength and impacts of atmospheric rivers. *Bulletin of the American Meteorological Society*, *100*(2), 269–289. https://doi.org/10.1175/BAMS-D-18-0023.1

Rauber, R. M., Hu, H., Dominguez, F., Nesbitt, S. W., McFarquhar, G. M., Zaremba, T. J., & Finlon, J. A. (2020). Structure of an atmospheric river over Australia and the Southern Ocean. Part I: Tropical and midlatitude water vapor fluxes. *Journal of Geophysical Research: Atmospheres*, *125*(18), e2020JD032513. https://doi.org/10.1029/2020JD032513

Rutz, J. J., Shields, C. A., Lora, J. M., Payne, A. E., Guan, B., Ullrich, P., et al. (2019). The atmospheric river tracking method intercomparison project (ARTMIP): Quantifying uncertainties in atmospheric river climatology. *Journal of Geophysical Research: Atmospheres*, *124*(24), 13777–13802. https://doi.org/10.1029/2019JD030936

Schmetz, J., PiliTjemkes, P. S., Just, D., Kerkmann, J., Rota, S., & Ratier, A. (2002). An introduction to meteosat second generation (MSG). *Bulletin of the American Meteorological Society*, *83*(7), 977–992. https://doi.org/10.1175/1520-0477(2002)083<0977:AITMSG>2.3.CO;2

Shields, C. A., & Kiehl, J. T. (2016). Atmospheric river landfall-latitude changes in future climate simulations. *Geophysical Research Letters*, *43*(16), 8775–8782. https://doi.org/10.1002/2016GL070470

Shields, C. A., Payne, A. E., Shearer, E. J., Wehner, M. F., O'Brien, T. A., Rutz, J. J., et al. (2023). Future atmospheric rivers and impacts on precipitation: Overview of the ARTMIP Tier 2 high-resolution global warming experiment. *Geophysical Research Letters*, *50*(6), e2022GL1029091. https://doi.org/10.1029/2022GL102091

Shields, C. A., Rutz, J. J., Leung, L.-Y., Ralph, F. M., Wehner, M., Kawzenuk, B., et al. (2018). Atmospheric river tracking method intercomparison project (ARTMIP): Project goals and experimental design. *Geoscientific Model Development*, *11*(6), 2455–2474. https://doi.org/10.5194/gmd-11-2455-2018

Shields, C. A., Willie, J. D., Marquardt Collow, A. B., Mclennan, M., & Gorodetskaya, I. V. (2022b). Evaluating uncertainty and modes of variability for Antarctic atmospheric rivers. *Geophysical Research Letters*, *49*(16), e2022GL099577. https://doi.org/10.1029/2022GL099577

Skamarock, W. C., Klemp, J. B., Dudhia, J., Gill, D. O., Liu, Z., Berner, J., et al. (2019). Description of the advanced research WRF model version 4.3 (No. NCAR/TN-556+STR). Retrieved from https://opensky.ucar.edu/islandora/object/opensky:2898

Stein, A. F., Draxler, R. R., Rolph, G. D., Stunder, B. J. B., Cohen, M. D., & Ngan, F. (2015). NOAA's HYSPLIT atmospheric transport and dispersion modeling system. *Bulletin of the American Meteorological Society*, *96*(12), 2059–2077. https://doi.org/10.1175/BAMS-D-14-00110.1

Taraphdar, S., Pauluis, O., Xue, L., Liu, C., Rasmussen, R., Ajayamohan, R. S., et al. (2021). WRF gray zone simulations of precipitation over the Middle-East and the UAE: Impacts of physical parameterizations and resolution. *Journal of Geophysical Research: Atmospheres*, *126*(10), e2021JD034648. https://doi.org/10.1029/2021JD034648

Tian, Y., Zhao, Y., Son, S.-W., Luo, J.-J., Oh, S.-G., & Wang, Y. (2023). A deep-learning ensemble method to detect atmospheric rivers and its application to projected changes in precipitation regime. *Journal of Geophysical Research: Atmospheres*, *128*(12), e2022JD037041. https://doi.org/10.1029/2022JD037041

Tsvieli, Y., & Zangvil, A. (2007). Synoptic climatological analysis of Red Sea Trough and non-Red Sea Trough rain situations over Israel. *Advances in Geosciences*, *12*, 137–143. https://doi.org/10.5194/adgeo-12-137-2007

Vallejo-Bernal, S. M., Wolf, F., Boers, N., Traxi, D., Marwan, N., & Kurths, J. (2023). The role of atmospheric rivers in the distribution of heavy precipitation events over North America. *Hydrology and Earth System Sciences*, *27*(14), 2645–2660. https://doi.org/10.5194/hess-27-2645-2023

van der Linden, R., Fink, A. H., Pinto, J. G., Phan-Van, T., & Kiladis, G. N. (2016). Modulation of daily rainfall in Southern Vietnam by the Madden-Julian Oscillation and convectively coupled equatorial waves. *Journal of Climate*, *29*(16), 5801–5820. https://doi.org/10.1175/JCLI-D-15-0911.1

Visbeck, M. H., Hurrell, J. W., Polvani, L., & Cullen, H. M. (2001). The North Atlantic Oscillation: Past, present, and future. *Proceedings of the National Academy of Sciences*, *98*(23), 12876–12877. https://doi.org/10.1073/pnas.231391598

Voss, K. K., Evant, A. T., & Ralph, F. M. (2021). Evaluating the meteorological conditions associated with dusty atmospheric rivers. *Journal of Geophysical Research: Atmospheres*, *126*(24), e2021JD035403. https://doi.org/10.1029/2021JD035403

Wallace, J. M., & Hobbs, P. V. (2006). *Atmospheric science, second edition: An introductory survey (international geophysics)* (p. 504). Academic Press.

Wang, H.-R., Li, F.-F., Grigorev, G. V., Yao, Z.-Y., Ge, D., Wang, G.-Q., & Qiu, J. (2024). Occurrence frequency of global Atmospheric River (AR) events: A data fusion analysis of 12 identification data sets. *Journal of Geophysical Research: Atmospheres*, *129*(5), e2023JD039730. https://doi.org/10.1029/2023JD039730

Wang, S., Ma, X., Zhou, S., Wu, L., Wang, H., Tang, Z., et al. (2023). Extreme atmospheric rivers in a warming climate. *Nature Communications*, *14*(1), 3219. https://doi.org/10.1038/s41467-023-38980-x

Wang, Z., Walsh, J., Szymborski, S., & Peng, M. (2020). Rapid Arctic Sea Ice loss on the synoptic time scale and related atmospheric circulation anomalies. *Journal of Climate*, *33*(5), 1597–1617. https://doi.org/10.1175/JCLI-D-19-0528.1

Wille, J. D., Alexander, S. P., Amory, C., Baiman, R., Barthelemy, L., Bergstrom, D. M., et al. (2024a). The extraordinary March 2022 East Antarctica "heat" wave. Part I: Observations and meteorological drivers. *Journal of Climate*, *37*(3), 757–778. https://doi.org/10.1175/JCLI-D-23-0175.1

Wille, J. D., Alexander, S. P., Amory, C., Baiman, R., Barthelemy, L., Bergstrom, D. M., et al. (2024b). The extraordinary March 2022 east Antarctica "heat" wave. Part II: Impacts on the Antarctic ice sheet. *Journal of Climate*, *37*(3), 779–799. https://doi.org/10.1175/JCLI-D-23-0176.1

WRF. (2023). Weather research and forecasting model [Software]. *GitHub*. Retrieved from https://github.com/wrf-model/WRF/releases

Yang, Y., Zhao, T., Ni, G., & Sun, T. (2018). Atmospheric rivers over the Bay of Bengal lead to northern Indian extreme rainfall. *International Journal of Climatology*, *38*(2), 1010–1021. https://doi.org/10.1002/joc.5229

Zhang, P., Chen, G., Ting, M., Leung, L. R., Guan, B., & Li, L. (2023). More frequent atmospheric rivers slow the seasonal recovery of Arctic sea ice. *Nature Climate Change*, *13*(3), 266–273. https://doi.org/10.1038/s41558-023-01599-3

Zhou, Y., Kim, H., & Guan, B. (2018). Life cycle of atmospheric rivers: Identification and climatological characteristics. *Journal of Geophysical Research: Atmospheres*, *123*(22), 12715–12725. https://doi.org/10.1029/2018JD029180

Zhu, Y., & Newell, R. (1998). A proposed algorithm for moisture fluxes from atmospheric rivers. *Monthly Weather Review*, *126*(3), 725–735. https://doi.org/10.1175/1520-0493(1998)126<0725:APAFMF>2.0.CO;2